Chinese Chemical Letters 32 (2021) 3457–3462

Contents lists available at ScienceDirect

Chinese Chemical Letters

journal homepage: www.elsevier.com/locate/cclet

Communication

Accelerated plasma degradation of organic pollutants in milliseconds and examinations by mass spectrometry

Hua Lu[a], Yiyan Yin[a], Jianghui Sun[a], Weixiang Li[a], Xiaotong Shen[b], Xiujuan Feng[c], Jin Ouyang[a], Na Na[a,*]

[a] Key Laboratory of Radiopharmaceuticals, Ministry of Education, College of Chemistry, Beijing Normal University, Beijing 100085, China
[b] School of Life Science, Beijing Institute of Technology, Beijing 100081, China
[c] School of Mines, China University of Mining & Technology, Beijing 100085, China

ARTICLE INFO

Article history:
Received 15 March 2021
Revised 26 April 2021
Accepted 31 May 2021
Available online 5 June 2021

Keywords:
Accelerated plasma degradation
Organic pollutants
Milliseconds
Intermediates
Ambient mass spectrometry
Degradation Mechanisms

ABSTRACT

The rapid degradation of organic pollutants, process monitoring and online controlling to obtain advanced products and decreased by-products are great and challenging tasks in environmental treatments. Herein, an accelerated plasma degradation in milliseconds was achieved by combining electrospray-based acceleration and plasma-based degradation. Taking the degradation of chloroaniline as an example, 97% of the degradation can be achieved in milliseconds. The velocity distribution of droplets was determined to be 40–50 m/s after being degraded for 0.30 ms, which exhibited different degradation behaviors in different milliseconds. Simultaneously, by virtue of the real-time and on-line detection ability of ambient mass spectrometry, intermediates, by-products and advanced products were monitored. Therefore, degradation mechanisms for different degradation times were proposed, which would provide theoretical guidance on obtaining efficient and green degradation. The fabrication, examining and understanding of accelerated plasma degradation not only enlarged application of accelerated reactions, but also promoted green and efficient degradation for environmental treatments.

With the continuous development of society and industry, degradation of various organic pollutants comes to be great and challenging tasks for the diversity of pollutants including volatile organic compounds, aromatic compounds, phenols or their derivatives [1-4]. Among efforts on pollutant degradation, plasma degradation contributes to faster, simpler, more efficient and green degradation than traditional methods [5-7]. As the “fourth matter” after solid, liquid and gas, plasma contains high-energy electrons, excited atomic molecules and other active particles [8-10]. Therefore, the organic pollutants in the plasma field would be endowed with powerful activities for oxygenolysis such as efficient dehalogenation or C=C bond fission. Nevertheless, the plasma degradation is still at preliminary development stage, whose process could not be well examined for great difficulties on online monitoring and controlling in millisecond time-scale [11]. Therefore, the online examining, monitoring and controlling of the plasma degradation are major determinants for the fast and efficient degradation with low toxic intermediates or products.

The traditional monitoring or characterizations on pollutant degradations are normally employed by optical techniques, such as ultraviolet absorption [12-14], fluorescence [15,16] and nuclear magnetic resonance spectroscopy methods [17]. In comparison, ambient mass spectrometry (AMS) is a powerful technique to directly and rapidly obtain molecular information without sample pre-treatment [18-20]. Recently, AMS has been successfully applied to observe reaction intermediates for mechanism studies [21-23]. Interestingly, the acceleration by electrospray (ESI) has become a new focus on organic reactions in confined-volume of solutions, which was evaluated by following on-line mass spectrometry [23-25]. Therefore, ESI-based AMS techniques have exhibited great potentials on both degradation acceleration and intermediate examinations for mechanism studies [26].

Herein, an accelerated plasma degradation (APD) system was constructed by the combination of ESI-based acceleration and plasma-based degradation. Chloroaniline was selected as a mode to study the degradation performance in milliseconds. By virtue of the real-time examination of AMS, an *in-situ* detection system of AMS was fabricated to observe and monitor important species during the APD. The instantaneous changes in milliseconds were

* Corresponding author.
E-mail address: nana@bnu.edu.cn (N. Na).

https://doi.org/10.1016/j.cclet.2021.05.074
1001-8417/

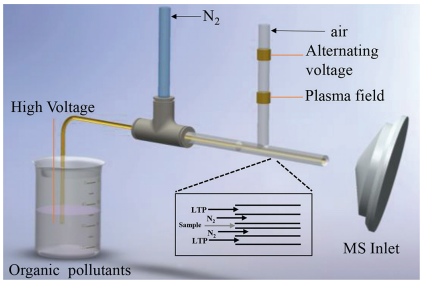

Fig. 1. Schematic diagram of plasma degradation and AMS systems.

firstly recorded, which provided significant information to propose APD mechanisms.

As shown in Fig. 1, the APD system is a three-layer of multiphase flow: the innermost pollutant solution, the interlayer N_2 nebulizing stream and the external gaseous plasma. The external plasma is generated by dielectric barrier discharge, whose configuration is designed based on our previous works [21,27]. The configuration consists of two high-voltage connected to copper electrodes, which were attached to the external surface of a quartz tube (i.d. 3.0 mm, o.d. 6.0 mm). With high voltage applied on, the electron avalanche is created between electrodes, while charged particles accumulate on the dielectric barrier to form wall charges. The electric field of wall charges always opposes the applied field, which triggered quenching of electron avalanches. While the high voltage is an alternating volage, which makes the applied electric field reversable to initiate the subsequent electron avalanche and quenching [28]. Therefore, the plasma is nonequilibrium with numerous microdischarges to generate high energy electrons, radicals, ions and metastable species. In our experiment, in the air flow, the plasma is generated between two electrodes under an alternating high-voltage powered with an 8 W-power supply. The generated plasma would be subsequently delivered down-flow and out of the quartz tube. It should be noted, although the average temperature of high-energy electrons in plasma is very high, the actual plasma gas temperature is close to the environment temperature [29]. Therefore, in the present sprayed system, the capillary would not be affected by plasma.

As illustrated, the organic pollutant solution is extracted and ultrasonically sprayed by an interlayer nebulizing stream of N_2 gas (5 L/min). This N_2 gas flows through a quartz tube (i.d. 1.0 mm, o.d. 0.7 mm), which covers an innermost quartz capillary (i.d. 0.52 mm, o.d. 0.69 mm). The innermost capillary is inserted directly into the organic pollutant solution, which is connected to a 3 kV high voltage for accelerated degradations. Simultaneously, bursts of charged droplets are generated to accelerate reactions. Thereafter, out of the quartz tube, the sprayed pollutants entered the plasma field for the accelerated plasma degradation. Meanwhile, the electromagnetic induction from dielectric barrier discharge would generate high electric fields between two electrodes and in downstream of discharge area out of quartz tube [30-32]. Then, bursts of charged droplets from the ESI would enter this field for the plasma degradation and accelerated by ESI. More significantly, high densities of charges in the small droplets would endow organic molecules with high reactivity [33], which accelerates the degradation by plasma. Significantly, the important species during the degradation would be ionized under the combination of ESI and plasma for MS detections. Fortunately, this type of on-line ionization can be considered as an AMS technique for detection of molecules with different polarities [21,34].

To examine the role of APD in degradation organic pollutants, 4-Cl-*o*PD was selected as the mode for examinations. As demonstrated in Fig. 2A, traditional ESI-based mass spectrometry only exhibits simple detection role to show positive molecular ions of $[4\text{-Cl-}o\text{PD} + H]^+$ at *m/z* 143. Fig. 2B shows that *via* the home-built ESI-based extraction under ultrasonic spray, 4-Cl-*o*PD in solution can be well extracted and detected. Moreover, with high-voltage of ESI applied on (Fig. 2C), the ionization efficiency is further increased. Although the accelerated reactions have been reported by ESI [35], there is still no significant degradation species of 4-Cl-*o*PD observed in this system. Therefore, without plasma, the ESI shows no obvious degradation ability.

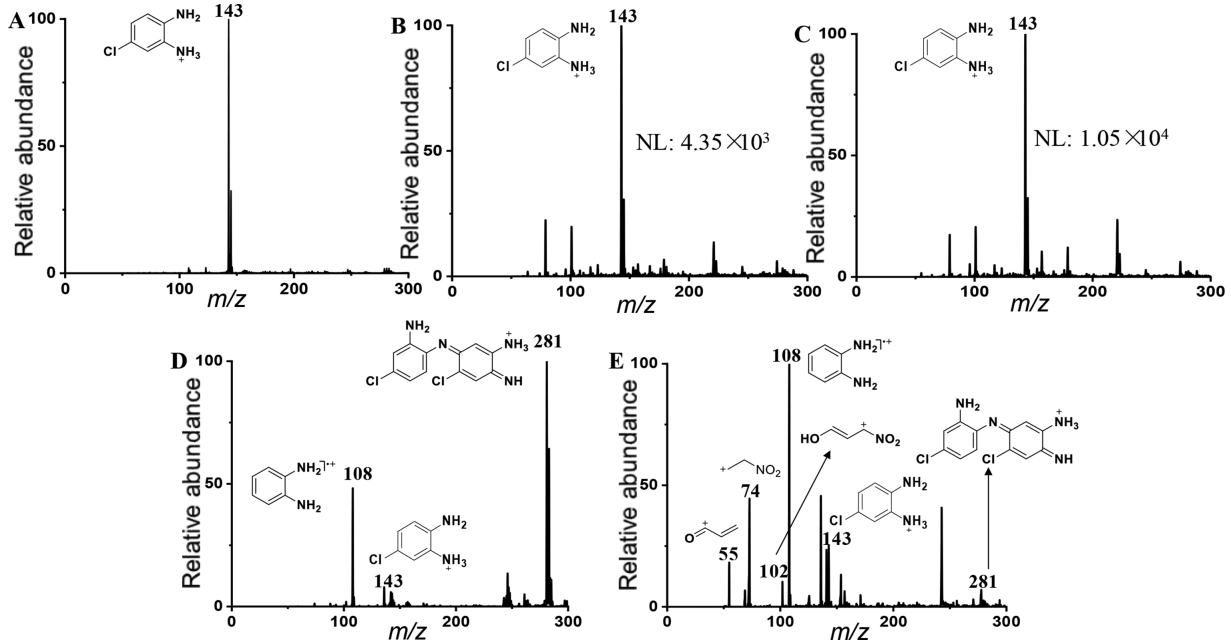

Fig. 2. The role of accelerated plasma degradation for the pollutant solution of 4-Cl-*o*PD. 1: The dimer of 4-Cl-*o*PD. 4-Cl-*o*PD concentration: 50 μmol/L. Plasma flow: 50 L/h. NL: Normalization level. (A) The detection of 4-Cl-*o*PD by traditional ESI-MS. (B) The extraction of samples from degradation system. (C) The extraction of samples from degradation system with high DC voltage applied on. (D) The degradation of 4-Cl-*o*PD in plasma field without high DC voltage applied on. (E) The degradation of 4-Cl-*o*PD in plasma field with high DC voltage applied on.

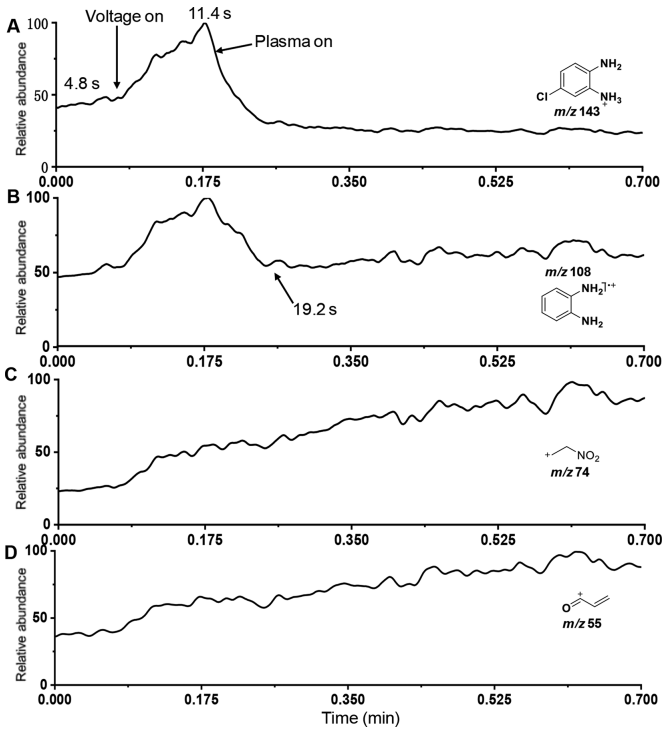

Fig. 3. Real-time monitoring of the accelerated plasma degradation of 4-Cl-*o*PD (50 μmol/L). (A) The ion of [4-Cl-*o*PD + H]$^+$ (*m/z* 143). (B) The ion of [*o*PD]$^+$ at *m/z* 108. (C) The ion of **[3]**$^+$at *m/z* 74. (D) The ion of **[2]**$^+$ at *m/z* 55.

However, by introducing bursts of charged pollutant species into plasma field, the degradation of pollutants was initiated, no matter whether the high-voltage of ESI was applied on or not. As shown in Fig. 2D, without high-voltage of ESI, the sprayed species of extracted pollutants can be degraded in plasma field, showing the dramatically decreased pollutant molecular ion of [4-Cl-*o*PD + H]$^+$ (*m/z* 143). Simultaneously, significantly increased ions of degradation species were observed, including the dechlorinated ion of [*o*PD]$^{\bullet+}$ at *m/z* 108 and the dimer ion of [**6** + H]$^+$ at *m/z* 281. It should be noted, with the high-voltage of ESI applied on, the reactivity of plasma degradation can be enhanced to accelerate the reaction, which results more degradation species. As shown in Fig. 2E, except for [*o*PD]$^{\bullet+}$, more degradation species including ions of **[1]**$^{\bullet+}$ at *m/z* 102, **[2]**$^{\bullet+}$ at *m/z* 55, **[3]**$^{\bullet+}$ at *m/z* 74 and by-product dimer ion of [**6** + H]$^+$ at *m/z* 281 were well detected. The structural information of these ions were further confirmed by collision induced dissociation (CID) experiments (Fig. S1 in Supporting information). Therefore, the organic pollutant can be degraded in the plasma field, which can be further accelerated by the ESI.

To examine dynamic changes of aforementioned species, the real-time and on-line monitoring of APD have been employed by AMS. During this process, the reactant ions of [4-Cl-*o*PD + H]$^+$ (*m/z* 143), and the degradation species of [*o*PD]$^{\bullet+}$ at *m/z* 108, **[2]**$^{\bullet+}$ at *m/z* 55 and **[3]**$^{\bullet+}$ at *m/z* 74 were monitored. As shown in Fig. 3A, the simple extraction of pollutant *via* N_2 nebulizing flow can result the ionized reactant of [4-Cl-*o*PD + H]$^+$ at *m/z* 143. While with the high-voltage of ESI applied on (at 4.8 s), the signal of [4-Cl-*o*PD + H]$^+$ increased dramatically, due to the increased ionization efficiency by ESI. Subsequently, with the plasma applied (11.4 s), the ion of [4-Cl-*o*PD + H]$^+$ decreased dramatically to the lowest values in 11 s (from 0.175 min to 0.35 min). Therefore, it can be demonstrated that the pollutants can be degraded rapidly by the present accelerated plasma degradation.

Interestingly, with ESI high voltage and plasma applied on (Fig. 3B), the dechlorinated ions of [*o*PD]$^{\bullet+}$ (*m/z* 108) showed similar changes to [4-Cl-*o*PD + H]$^+$ (*m/z* 143) at the beginning. However, when both the reactant ion (*m/z* 143) and the dechlorinated ions of [*o*PD]$^{\bullet+}$ (*m/z* 108) decreased to the lowest value at about 19.2 s, the ions of [*o*PD]$^{\bullet+}$ increased slightly. This could be generated from the fast accumulation of [*o*PD]$^{\bullet+}$ by dechlorination of 4-Cl-*o*PD. Subsequently, the advanced degradation after dechlorination was further conducted to obtain smaller degradation species. This is further confirmed by the increased signals of **[2]**$^{\bullet+}$ at *m/z* 55 and **[3]**$^{\bullet+}$ at *m/z* 74 (Figs. 3C and D).

During APD, except for the advanced degradation products of small molecules, some by-products were also observed. For example, Fig. 2E recorded the dimer ion of [6 + H]$^+$ at *m/z* 281. As monitored (Fig. S2A in Supporting information), with the ESI high voltage (4.8 s) and plasma applied on (11.4 s), the dimer ion (*m/z* 281) shows similar changes to [4-Cl-*o*PD + H]$^+$ (*m/z* 143). Differently, the signal intensity of the dimer at *m/z* 281 came to be stable thereafter. This might be due to the kinetic equilibrium between dimer formation and subsequently reversible reactions. The dimer structure was confirmed by CID experiments (Figs. S2B-D in Supporting information). Thus, although the signal of original pollutant decreased dramatically, it could not be a real efficient degradation due to the possibility on generating pollutants of by-products. Therefore, the control of accelerated plasma degradation is crucial to obtain real advanced degradation of pollutants.

Considering the important role of plasma for the present degradation, the plasma flow was firstly examined. Here, different flows of the plasma were obtained by changing the flow rates of air during dielectric barrier discharge. As shown in Fig. 4A, both [4-Cl-*o*PD + H]$^+$ at *m/z* 143 and by-product ion at *m/z* 281 decreased with increasing the plasma flow. As demonstrated, ion signal intensities of pollutant and dimer decreased with increasing plasma flow (Fig. 4B), which obtained 97% of degradation efficiency at 80 L/h of plasma (the inset of Fig. 4B). Therefore, the degradation can be controlled by changing plasma flow, which not only affects the degradation efficiency of the reactant, but also suppresses the by-product generation.

Furthermore, we found the configuration of quartz tubes also affected the accelerated plasma degradation. Fig. 5 shows the degradation of 4-Cl-*o*PD by different configuration of quartz tubes. Compared to the degradation with the inner quartz tube extended outside (Fig. 5A), we obtained advanced degradation with quartz tubes cut evenly (Fig. 5B). Obviously, no pollutant ion of 4-Cl-*o*PD (*m/z* 143) was observed with the inner tube cut evenly. In addition, more degradation products with increased signals, including ions of **[2]**$^{\bullet+}$ at *m/z* 55 and **[3]**$^{\bullet+}$ at *m/z* 74, were recorded. Furthermore, as the dechlorinated ion of [*o*PD]$^{\bullet+}$ at *m/z* 108 decreased, more advanced degradation product of [**5** + H]$^+$ at *m/z* 91 was observed and came to be the main ion peak in the spectrum. This could be generated from different linear velocities of N_2 when contacting with droplets out of the internal capillary. Thus, different sizes of droplets could be obtained to exhibit different behaviours of accelerated degradations with different surface tension, conductivity and relative permittivity [36]. Therefore, the design of the configurations can also affect the accelerated plasma degradation.

Considering the great changes could occur instantly during the pollutant spray, time dependent profiles of the accelerated plasma degradation were collected. The degradation time was calculated based on the linear velocity and travelling distance of droplets. Measured by a PIV system, the linear velocity was measured to obtain a velocity distribution. Video S1 (Supporting information) showed the magnified spray in a slow motion, which was recorded by PIV under a microscope equipped with an illuminating laser. As shown in Fig. 6A, the sprayed droplets showed different velocity distribution out of the tip of the quartz tube. In

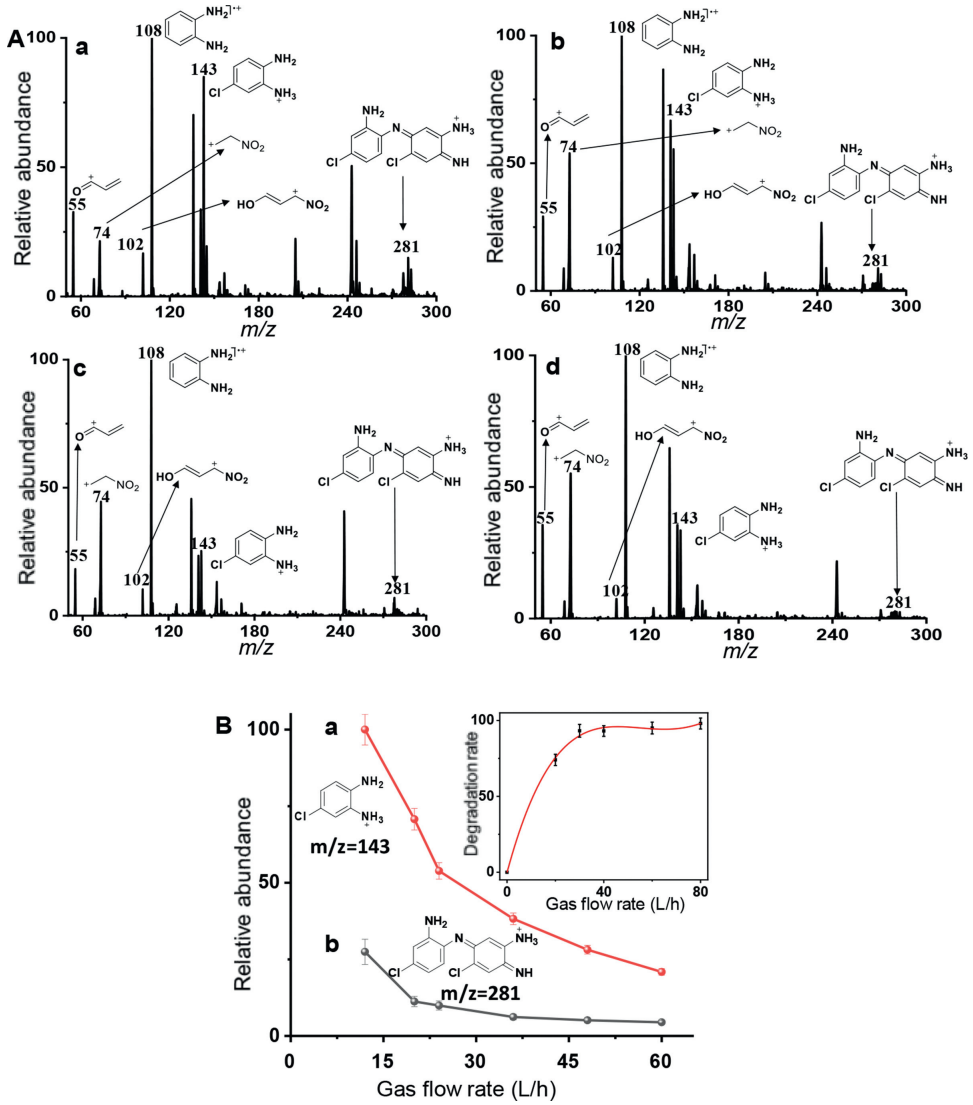

Fig. 4. Plasma flow for controlling the accelerated plasma degradation. (A) Mass spectra of at different plasma flow. (a) 20 L/h, (b) 30 L/h, (c) 40 L/h, (d) 60 L/h. 4-Cl-oPD concentration: 50 μmol/L. (B) Signal intensity of pollutant ion of *m/z* 143 (a) and dimer ion of *m/z* 281 (b) as a function of plasma flow. The inset: The changes of the degradation rate as a function of gas flow rate.

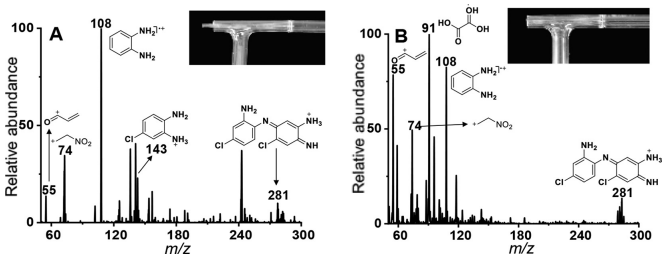

Fig. 5. Comparison of the degradation with or without the inner quartz tube even cut. (A) The mass spectrum with the inner tube even cut. (B) The mass spectrum without the inner tube even cut. The insets are the pictures of two kinds of quartz tubes.

X-axis direction, the velocity of the droplets first increased after sprayed out of the quartz tube and then decreased. In Y-axis direction, the velocity decreased dramatically and symmetrically away from the sprayed tip. In the experiment, the reaction time can be calculated according to the sprayed distance and the accurate speed measured by PIV. Therefore, the relative high velocity of 40–50 m/s is obtained after being degraded for approximately 0.30 ms. The highest velocity emerges at about 20 mm away from the sprayed tip in X-direction (Fig. 6A-b). Therefore, different degradation times were obtained at different locations, which would have great effects on the performance of accelerated plasma degradation.

To examine the performance of degradation for different times, mass spectra of 4-Cl-oPD degraded for 0.15 ms, 0.30 ms, 1.60 ms were collected, respectively. While as the degradation carried on, the signal intensities of observed products changed distinctively (Fig. S3 in Supporting information). Furthermore, we also recorded new degradation ion of **[4]**$^{\bullet+}$ at *m/z* 88 (Fig. 6B-b), whose structure was confirmed by CID experiments (Fig. S4A in Supporting information). In addition, the dimer ion at *m/z* 281 increased by further prolonging the degradation time (Fig. 6B-c). Therefore, although we obtained efficient degradation with no obvious reactant observed, the degradation degrees at different times were still different. More degradation products including some by-products would be obtained after the relative longer degradation.

In this system, large amounts of active species such as ozone and high energy electrons exhibited important roles [37]. The possible mechanism for the accelerated plasma degradation was pro-

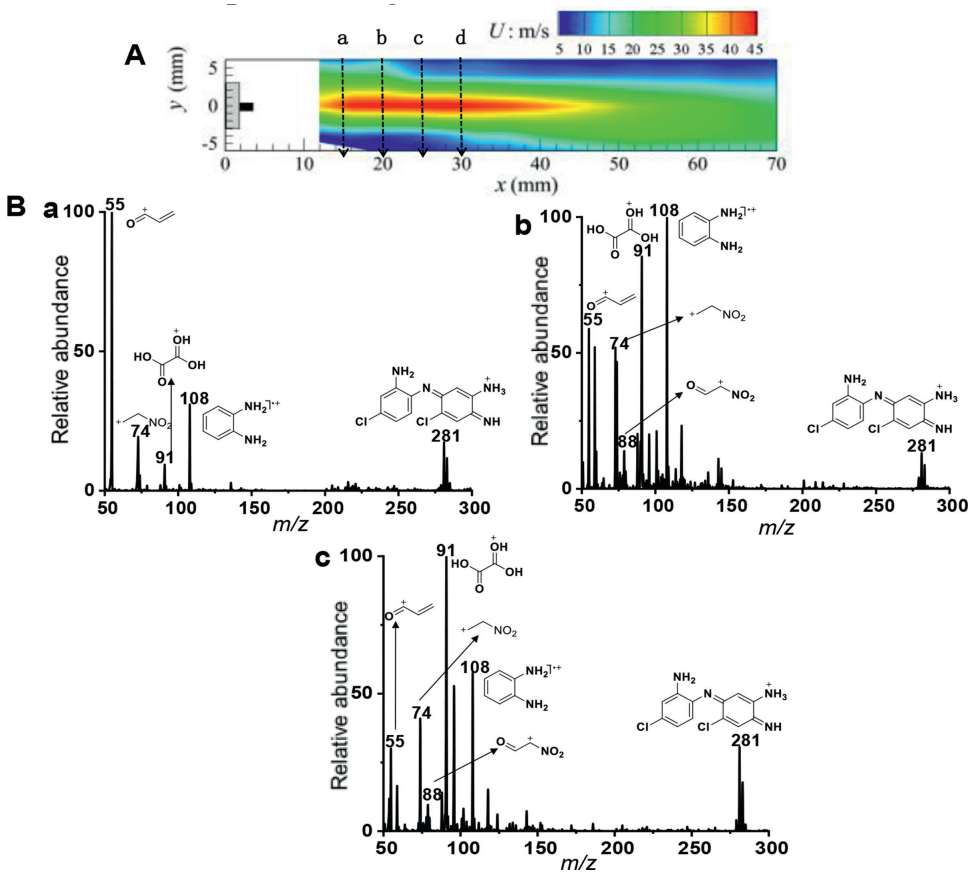

Fig. 6. The performance of accelerated plasma degradation at different times. (A) The velocity distribution by PIV measurement. The degradation time for different location: (a) 0.15 ms, (b) 0.30 ms, (c) 0.45 ms, (d) 1.60 ms. (B) Mass spectra after degradation for (a) 0.15 ms, (b) 0.30 ms and (c) 1.60 ms.

posed based on the molecular information obtained by the online detection of AMS. Herein, to obtain more structural information, the degradation products were also monitored by AMS in the negative ion mode. As demonstrated in Fig. S4B (Supporting information), we recorded product ions of $[CO_3]^{\bullet-}$ at *m/z* 60, $[NO_3]^-$ at *m/z* 62, $[CO_3 \cdot HNO_3]^{\bullet-}$ at *m/z* 123 and $[HNO_3 \cdot NO_3]^-$ at *m/z* 125. The structural of these anions have been confirmed by both CID experiments and some reports [8,38-40]. Furthermore, the final advanced degradation product of CO_2 was confirmed by the precipitation experiment with exhaust gas introduced into $Ca(OH)_2$ solution (Fig. S5 in Supporting information). The recorded ions confirmed the obtaining of advanced degradation products including carbonate and nitrate. Therefore, based on structural information of degradation products at different degradation degree, different routes including Route Dechlorination and Route Cyclization were proposed.

As shown in Fig. 7, in route dechlorination, the direct dechlorination product of *o*PD radical is first obtained (at *m/z* 108). Subsequently, in the presence of O_3 from the plasma, *o*PD radicals are oxidized into *o*-nitrobenzene (MW 168), in accordance with the reports [8]. Thereafter, three routes of ring cleavages occur in the plasma field full of O_3. In detail, in ring cleavage I, homolytic cleavage of *o*-nitrobenzene (into two parts) occurs to obtain Product **1** (shows the ion at *m/z* 102). Then, the more advanced products of **2** and **3** at *m/z* 74 and *m/z* 55 are generated, which result the product ions of NO_3^- and $CO_3^{\bullet-}$ or CO_2. Similarly, in ring cleavage II and III, **4** and **5** are generated under the oxidation of O_3, both of which result final products of CO_2, H_2O and $NO_3^{\bullet-}$. In addition, the reversible cyclization reaction is also a side reaction of the degradation to form the dimer of **6**, which has been confirmed by the observed ions at *m/z* 281.

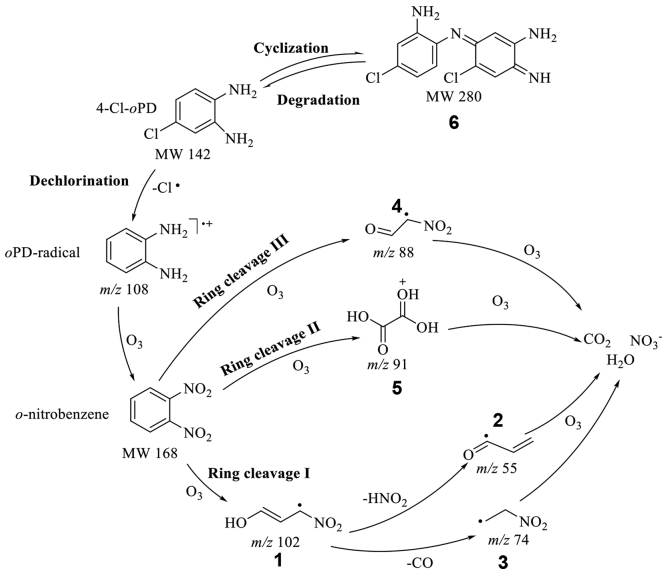

Fig. 7. Schematic diagram of the possible mechanism for the accelerated plasma degradation of 4-Cl-*o*PD.

In conclusion, the APD in milliseconds is constructed and examined by ambient mass spectrometry. The pollutants can be efficiently degraded in milliseconds, whose products are controlled and monitored on different conditions of APD. Furthermore, based on fast changes on pollutant structures recorded by on-line MS detection, important species and the advanced products are well ex-

amined. Therefore, possible routes have been proposed to demonstrate degradation behaviors in milliseconds, which is favorable for product controls. The present fabrication and examination on the accelerated plasma degradation would provide potentials for rapid, efficient, green and controllable degradation for environmental treatments.

Declaration of competing interest

We declare that we have no financial and personal relationships with other people or organizations that can inappropriately influence our work.

Acknowledgments

The authors gratefully acknowledge the financial support provided by the National Key Research and Development Program of China (No. 2019YFC1805600) and the National Natural Science Foundation of China (Nos. 21874012, 21974010).

Supplementary materials

Supplementary material associated with this article can be found, in the online version, at doi:10.1016/j.cclet.2021.05.074.

References

[1] S. Zhang, J. You, C. Kennes, et al., Chem. Eng. J. 334 (2018) 2625–2637.
[2] U. Poeschl, M. Shiraiwa, Chem. Rev. 115 (2015) 4440–4475.
[3] C. He, J. Cheng, X. Zhang, et al., Chem. Rev. 119 (2019) 4471–4568.
[4] Y. Dumanoglu, M. Kara, H. Altiok, et al., Atmos. Environ. 98 (2014) 168–178.
[5] Y. Guo, X. Liao, M. Fu, et al., J. Environ. Sci. 28 (2015) 187–194.
[6] B. Lee, D.W. Kim, D.W. Park, Chem. Eng. J. 357 (2019) 188–197.
[7] B.W. Wang, G.H. Xu, Chin. Chem. Lett. 14 (2003) 316–318.
[8] W. Sang, J. Cui, Y. Feng, et al., Chemosphere 223 (2019) 416–424.
[9] Y. Shu, M. He, J. Ji, et al., J. Hazard. Mater. 364 (2019) 770–779.
[10] A. George, B. Shen, M. Craven, et al., Renew. Sustain. Energy Rev. 135 (2021) 109702–109724.
[11] B.W. Wang, G.H. Xu, Chin. Chem. Lett. 14 (2003) 1236–1238.
[12] X. Zhang, B. Gao, Y. Zheng, et al., Bioresource Technol. 245 (2017) 606–614.
[13] X. Zhang, B. Gao, A.E. Creamer, et al., J. Hazard. Mater. 338 (2017) 102–123.
[14] I. Vassalini, G. Ribaudo, A. Gianoncelli, et al., Environ. Sci. Nano 7 (2020) 3888–3900.
[15] G. Liang, F. Ren, H. Gao, et al., ACS Sens. 1 (2016) 1272–1278.
[16] G. Liang, F. Ren, H. Gao, et al., J. Mater. Chem. A 5 (2017) 2115–2122.
[17] Q. Lin, X.-.W. Guan, Y.M. Zhang, et al., ACS Sustain. Chem. Eng. 7 (2019) 14775–14784.
[18] J. Han, Y. Li, L. Zhan, et al., Chem. Commun. 54 (2018) 10726–10729.
[19] C. Qi, H. Jiang, J. Xiong, et al., Chin. Chem. Lett. 30 (2019) 553–557.
[20] H.W. Xie, S.Y. Liu, L.X. Wang, Y.Q. Shun, Chin. Chem. Lett. 6 (1995) 403–406.
[21] Y. Wang, J. Sun, J. Qiao, et al., Anal. Chem. 90 (2018) 14095–14099.
[22] X. Yan, X. Li, C. Zhang, et al., J. Am. Soc. Mass Spectrom. 28 (2017) 1175–1181.
[23] Y.Q. Liu, H.H. Li, Y.H. Ye, G. Yuan, Chin. Chem. Lett. 20 (2009) 330–333.
[24] X. Yan, R.M. Bain, R.G. Cooks, Angew.Chem. Int. Ed. 55 (2016) 12960–12972.
[25] X. Yan, E. Sokol, X. Li, et al., Angew. Chem. Int. Ed. 53 (2014) 5931–5935.
[26] J.P. Sun, Q. Han, X.Q. Zhang, M.Y. Ding, Chin. Chem. Lett. 25 (2014) 1259–1264.
[27] Y. Wang, M. Sun, J. Qiao, et al., Chem. Sci. 9 (2018) 594–599.
[28] Y.M. Ling, Phys. Plasmas 12 (2005) 113504.
[29] J.D. Harper, N.A. Charipar, C.C. Mulligan, et al., Anal. Chem. 80 (2008) 9097–9104.
[30] J. Wu, Q. Xiong, J. Liang, et al., Chem. Eng. J. 384 (2020) 123300.
[31] N. Jiang, L. Guo, C. Qiu, et al., Chem. Eng. J. 350 (2018) 12–19.
[32] N. Jiang, C. Qiu, L. Guo, et al., J. Hazard. Mater. 369 (2019) 611–620.
[33] Z. Wei, Y. Li, R.G. Cooks, X. Yan, Annu. Rev. Phy. Chem. 71 (2020) 31–51.
[34] L. Zhang, X.X. Cao, H.X. Jiang, et al., Chin. Chem. Lett. 20 (2009) 716–719.
[35] W. Zhang, S. Yang, Q. Lin, et al., J. Org. Chem. 84 (2019) 851–859.
[36] C. Zhu, Y. Fu, Y. Yu, Adv. Mater. 31 (2019) 1803408.
[37] Z. Chang, C. Wang, G. Zhang, Plasma Process Polym 17 (2020) 1900131.
[38] C. Jiang, Y. Yang, L. Zhang, et al., J. Hazard. Mater. 400 (2020) 743–748.
[39] J. Pavlov, A.B. Attygalle, Anal. Chem. 85 (2013) 278–282.
[40] D. Smith, M.J. McEwan, P. Spanel, Anal. Chem. 92 (2020) 12750–12762.